Velocity Measurements in Cardiac Magnetic Resonance Imaging

Rolf, M.P.

2012

document version
Publisher's PDF, also known as Version of record

Chapter 3

3D velocity quantification in the heart: improvements by 3D PC-SSFP

Marijn P. Rolf, Mark B.M. Hofman, Joost P.A. Kuijer, Albert C. van Rossum, and Rob M. Heethaar

Published in *Journal of Magnetic Resonance Imaging* (2009) 30:5, pp. 947-955.

Abstract

Purpose: To test whether a 3D imaging sequence with phase contrast (PC) velocity encoding based on steady-state free precession (SSFP) improves 3D velocity quantification in the heart compared to the currently available gradient echo (GE) approach.

Materials and Methods: The 3D PC-SSFP sequence with 1D velocity encoding was compared at the mitral valve in 12 healthy subjects with 3D PC-GE at 1.5T. Velocity measurements, velocity-to-noise-ratio efficiency (VNR_{eff}), intra- and interobserver variability of area and velocity measurements, contrast-to-noise-ratio (CNR), and artifact sensitivity were evaluated in both long- and short-axis orientation.

Results: Descending aorta mean and peak velocities correlated well (r^2=0.79 and 0.93) between 3D PC-SSFP and 3D PC-GE. At the mitral valve, mean velocity correlation was moderate (r^2=0.70 short axis, 0.56 long axis) and peak velocity showed good correlation (r^2=0.94 short axis, 0.81 long axis). In some cases VNR_{eff} was higher, in others lesser, depending on slab orientation and cardiac phase. Intra- and interobserver variability was generally better for 3D PC-SSFP. CNR improved significantly, especially at end systole. Artifact levels did not increase.

Conclusion: 3D SSFP velocity quantification was successfully tested in the heart. Blood-myocardium contrast improved significantly, resulting in more reproducible velocity measurements for 3D PC-SSFP at 1.5T.

3.1 Introduction

Blood flow velocity measurement with phase-contrast magnetic resonance imaging (MRI) is a valuable tool used, for example, in cardiology. Flow measurements through the large vessels and heart valves can be useful for monitoring disease progression. Mitral valve regurgitation is an important risk factor for the development of heart failure; therefore, accurate measurements of the regurgitant fraction might help clinical decisions about treatment [1, 2].

In direct quantification of the regurgitant volume flow at the mitral valve, two specific issues play a role: movement of the valvular plane, for which correction is needed, and signal voids in the case of regurgitant jets [1, 3]. The use of moving slice imaging [4] handles the first issue, but not the second. The control volume approach [5] is a solution that could compensate for both of these issues. In this approach a control surface is drawn at the ventricular side of the regurgitant orifice. In every cardiac phase the control surface moves along with the mitral valve. The blood volume flowing perpendicular through this surface equals the mitral volume flow. However, this method requires a 3D acquisition with three-directional velocity encoding.

Velocity encoding is generally widely available with a spoiled gradient echo (GE) sequence [6–8]. Due to the short TRs used for fast imaging, in combination with the applied excitation angles, the signal is generally strongly dependent on the blood inflow [9, 10]. In 3D imaging, however, depending on the size and orientation of the volume relative to the heart and large vessels, blood-myocardium contrast can be considerably reduced [11, 12]. Especially during systole, when the mitral valve is closed, the contrast between blood and myocardium can drop significantly due to limited inflow. This makes it difficult to recognize and delineate the anatomy [13, 14]; in particular, it is more difficult to assess valvular plane motion, especially in systole, in cases of mitral regurgitation evaluation. Therefore, the control volume approach does not work well with 3D phase contrast (PC) GE images.

Better contrast is expected from a steady-state free precession

(SSFP) sequence [13]. The signal intensity of this sequence basically depends on the ratio of the T2 and T1 relaxation times, and the image contrast is less dependent on inflow, size, and orientation of the imaging volume. For cine imaging it has been shown that SSFP has better signal-to-noise ratio (SNR) and contrast-to-noise ratio (CNR) than spoiled GE in both 2D [11, 13] and 3D [12]. Phase contrast measurements using an SSFP sequence are still under research and have been reported for cardiac 2D acquisitions [15–17] and in the brain for 3D acquisitions [18]. From the three reported cardiac sequences, the one by Markl et al. [15] is, due to its intrinsic velocity encoding using the slice selection gradient, not suitable for extension to 3D imaging with three-directional velocity encoding. Using this method, the increase in TR would affect temporal resolution and artifact sensitivity, as was pointed out by Santini et al. [18]. The method proposed by Pai [17] is not suitable due to its sensitivity to artifacts [19]. Therefore, we have chosen to use the PC technique described by Overall et al. [16]. The extension to a 3D sequence with 3D velocity encoding is relatively straightforward for this method. In this study we implemented 1D velocity encoding in a 3D SSFP sequence on a 1.5T scanner. The 3D PC-SSFP sequence was evaluated against the currently available 3D PC-GE on velocity quantification at the mitral valve level. This comparison will make clear which of these 3D phase contrast methods is best suitable for use with the control volume approach.

3.2 Materials and Methods

Sequence

The 3D PC-SSFP sequence is based on a regular 3D SSFP gradient scheme with velocity encoding as introduced for 2D by Overall et al. [16]. After the readout a bipolar velocity-encoding pulse was placed on the slice-selection or read-out axis for through-plane or in-plane velocity encoding, respectively (Figure 3.1). To keep the two steady states for phase contrast imaging as similar as possible, the polarity of the bipolar pulses was alternated at each cardiac trigger for phase subtraction. In PC-GE the relation between image phase and veloc-

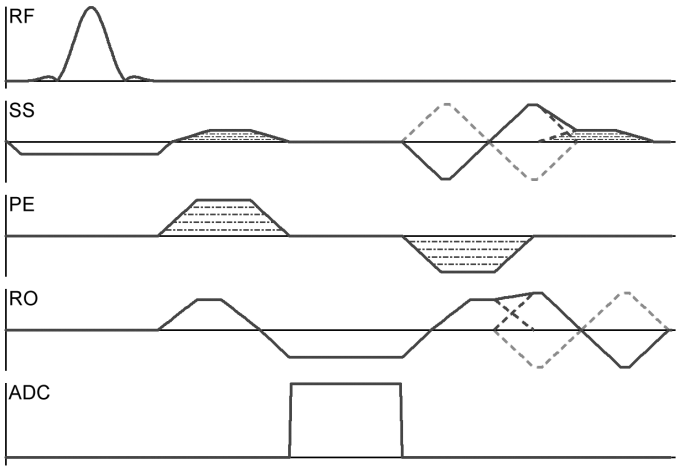

Figure 3.1: The 3D PC-SSFP sequence. The bipolar velocity encoding pulse can be placed on the slice-selection (SS) or on the read-out (RO) axis, for through-plane and in-plane velocity encoding, respectively. The sequence uses positive and negative velocity encoding (– – –). The different imaging encoding steps are shown by (– – –).

ity is linear for all phase angles. In PC-SSFP, the linear relationship between image phase and velocity is valid only over a finite range of phase angles. The largest velocity that can be measured in the linear range, is indicated by v_{max}, and is assumed to be $\pm v_{enc}/2$. This is caused by offresonance effects in SSFP in combination with some variation of B_O within the volume of interest (a more detailed explanation is provided by Overall et al. [16]). Because of the symmetry around the magnetization x-axis in the steady state, the signal phase (the angle between the magnetization and the x-axis) is only half the total velocity-induced phase. This phenomenon is referred to as the slope-1/2 approximation (a more detailed explanation is provided by Overall et al. [16]).

In this study 1D velocity encoding was used to keep acquisition times short enough to apply multiple comparisons in one subject. With the same principle 3D velocity encoding could be applied.

The 3D PC-SSFP sequence was implemented on a 1.5T scanner

(Magnetom Sonata, Siemens, Erlangen, Germany) with a gradient performance of 40 mT/m and 200 T/m·s.

In Vitro Measurements
The velocity quantification of the sequence was tested in a custom-made flow phantom. The phantom consisted of a Perspex cube with 15-cm-long edges, filled with stationary fluid. Inside the cube, fluid flowed through a tube with a diameter of 4.15 mm. The flow circuit was driven by a rotary vane pump (Procon, Murfreesboro TN), creating a steady flow. A float displacement volume flow meter (Brooksmeter model 1307, Brooks Instrument, the Netherlands) was mounted in the flow circuit and was calibrated for the actual viscosity of the phantom fluid. This setup could generate volume flow rates ranging up to 1.5 L/min (cross-sectional average velocity: 185 cm/s). The phantom fluid consisted of water with 0.9 mass percent NaCl for coil loading and 0.05 mmol/L MnCl2 to lower relaxation times (T1/T2/T2* 1505/204/198 msec, experimentally determined). To get a fluid viscosity comparable to blood ($\approx$ 3.5 mPa·s in the normal population [20]), methylcellulose (4000 cP 0.2 vol%) was added, resulting in a viscosity of 4 mPa·s. Measurements were performed at 14 different volume flow rates. PC-SSFP sequence parameters were: spatial resolution $1.3 \times 1.3 \times 8$ mm^3 matrix $128 \times 128 \times 8$, field of view (FOV) $162 \times 162 \times 64$ mm^3, v_{max} 150 cm/s, TR 4.3 msec, TE 1.76 msec, excitation angle 50°, bandwidth (BW) 1502 Hz/pix, and the body coil for RF receiving. PC-GE used v_{enc} 150 cm/s, TR 11 msec, TE 6.4 msec, excitation angle 20°, BW 190 Hz/pix; all other parameters were equal to those used in PC-SSFP.

In Vivo Measurements
The mitral valves of 12 healthy volunteers (six male, age 22 ± 4 years) were scanned with 3D PC-SSFP. Not all measurements were performed in all subjects due to local scanner time constraints. The study was approved by the local ethics committee and all subjects gave written informed consent. As direction of flow influences inflow enhancement and artifact sensitivity, the mitral valve was imaged in

two orientations: long axis and short axis, with in-plane and through-plane velocity sensitivity, respectively (Figure 3.2, top row). The same measurements were also performed using a conventional phase contrast spoiled gradient echo (3D PC-GE) [21–23]. Imaging parameters for both sequences were: spatial resolution $1.8 \times 1.8 \times 8$ mm^3, matrix $192 \times 132 \times 8$, FOV $340 \times 234 \times 64$ mm^3, prospective ECG gating, phased-array receiver coil, no parallel imaging. For PC-SSFP the settings were: TR 4.3 msec, TE 1.7 msec, 5 phase encoding steps per heartbeat, excitation angle 50°, BW 1530 Hz/pix, v_{max} 150 cm/s, temporal resolution 21.5 msec, and a locally adjusted shim; resulting in an acquisition time of 7 minutes at a heart rate of 60 beats per minute. For PC-GE the settings were: TR 11 msec, TE 6.6 msec, 1 phase encoding step per heartbeat, excitation angle 20°, BW 190 Hz/pix, v_{enc} 150 cm/s, and temporal resolution 22 msec; resulting in an acquisition time of 18 minutes at a heart rate of 60 beats per minute. Imaging was performed as the subjects breathed freely. PC-SSFP excitation angle was maximized to obtain optimal SNR, but was restricted by radiofrequency (RF) power amplifier, and at slightly higher excitation angles SAR limits would have been a limitation as well. These limitations are similar to those described in the literature [24, 25], with similar resulting excitation angles. The excitation angle of the PC-GE protocol was chosen similar to values reported in the literature [26, 27].

Data Analysis and Statistics

Flow Phantom

Cross-sectionally averaged velocity in the tube was measured in the 3D PC-SSFP and 3D PC-GE images using commercial software (Mass, Medis, Leiden, the Netherlands). Regions of interest (ROIs) were drawn with an area matching the known tube diameter to limit partial volume errors. Velocity offset was corrected by fitting a surface through the time average of stationary pixels of the phase images [28]; this was also done for the in vivo images. The measured velocities were then compared with velocities calculated from the volume flow meter readings. The validity of velocity measurements was tested by

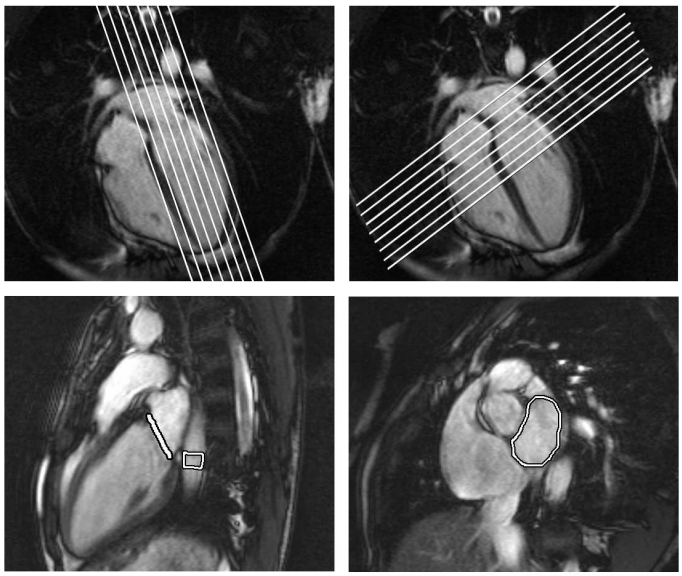

Figure 3.2: Top row: orientations of long-axis (left) and short-axis (right) volumes presented on a four chamber image. Bottom row: ROIs for velocity quantification in the middle slice of the 3D dataset (slice 4 or 5 of 8). Left: longaxis orientation with the line ROI for velocity at the mitral valve level and an ROI in the descending aorta for velocity validation. Right: short-axis orientation with ROI for velocity at the mitral valve level.

comparing the slope and intercept outcomes of linear regression with the line of identity.

Flow In Vivo

For further evaluation of the sequence, velocity measurements were performed in the descending aorta, which is imaged in the long-axis acquisitions. The descending aorta was chosen because of its uncomplicated anatomy and blood flow compared to the mitral valve. This makes the evaluation of the SSFP sequence in vivo less sensitive to contour drawing. ROIs covering the full cross-section of the descending aorta in all cardiac phases were drawn on the magnitude images

of a central slice of the 3D image set (Figure 3.2) using commercial software (Mass, Medis). The mean velocity in the ROI was then calculated for each cardiac phase. Next, the mean velocity over the whole cardiac cycle and the peak velocity were compared between 3D PC-SSFP and 3D PC-GE using a paired Students t-test and linear regression analysis. Velocity of blood flow through the mitral valve was compared in a similar way. ROIs were drawn in one of the middle slices from the 3D image set at the location of the mitral valvular annulus; in short-axis images by a circular shape, in long-axis images by a line (Figure 3.2). Subsequently, cross-sectional averaged velocities or line averaged values were determined. All image sets were analyzed twice by two observers. Analyses were performed in random order, with several days to weeks between the repeated analysis of the same dataset. Using the average result of the two analyses of each observer, the mean velocity over the cardiac cycle and peak velocity within the cardiac cycle were compared between the two sequences by a paired Students t-test and linear regression analysis. Reproducibility of each sequence was assessed by BlandAltman intra- and interobserver analyses of the average and peak velocities and short axis area. For the interobserver study the averaged results of the repeated analysis by each observer were used.

VNR and CNR

VNR and CNR calculations were based on signal magnitude measurements. Signal magnitude of blood was measured from an ROI in the left ventricle close to the mitral valve. Myocardial signal magnitude was measured in the muscle at the free wall of the left ventricle. Noise was measured as the standard deviation of signal magnitude in air outside the subject. A factor of 0.70 was applied to correct for noise measured in magnitude images from multiple receivers [29]. As signal magnitude is expected to depend on inflow, signal magnitudes were measured at two instances; in midsystole and at peak inflow in diastole. Mid-systole (in milliseconds) was defined as $273-1.05\times$ heart rate (beats/min) [24], and the averages of five cardiac phases around this timepoint were taken. The diastolic value was determined as the average of three phases around the peak in blood signal magni-

tude shortly after end-systole. Signal magnitude measurements were performed using commercial software (Mass, Medis).

The velocity-to-noise ratio (VNR) is indicated by the following relations [16, 30]:

$$VNR_{GE} = \sqrt{2} \cdot SNR \cdot \gamma \cdot 2 \cdot m_{1,GE} \cdot v_{enc} \tag{3.1}$$

$$VNR_{SSFP} = \sqrt{2} \cdot SNR \cdot \gamma \cdot 2 \cdot m_{1,SSFP} \cdot v_{max} \tag{3.2}$$

with SNR the signal-to-noise ratio in the magnitude image, γ the gyromagnetic ratio, m_1 the first gradient moment, and v the maximum velocity that can be reliably measured. The $\sqrt{2}$ is introduced by taking the phase difference. While the VNR differs by this factor $\sqrt{2}$ from the phase-to-noise ratio as defined by Overall et al. [16], VNR gives an absolute number that better represents the actual velocity map. The VNR of SSFP differs from the VNR of GE by a factor of 2, due to the slope-1/2 approximation. Consequently, the SNR of PC-SSFP has to be twice as high as for PC-GE in order to obtain equal VNR. VNR efficiency (VNR_{eff}) was defined as the VNR divided by the square root of scan time. CNR was defined as the signal magnitude difference between blood and myocardium divided by the noise level. Differences in VNR_{eff} and CNR between the two sequences were tested with the paired Students t-test.

Artifacts
Artifacts located at the ROI, eg, around the mitral valve, were visually scored on their severity on a 4-point scale from absent (0) to severe (3). All time series were scored three times in random order and an average score was used for comparative analysis by the Wilcoxon signed rank sum test.

3.3 Results

Sequence Testing
In vitro average velocities measured in the 3D PC-SSFP velocity maps were plotted against velocities calculated from the volume flow meter

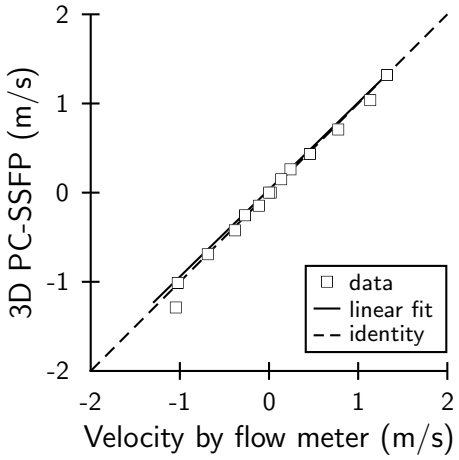

Figure 3.3: In vitro comparison: cross-sectional averaged velocity measured with 3D PC-SSFP against flow meter readings. Data were consistent with the line of identity (slope 0.98 P=0.39, offset 0.03 m/s P=0.1), and the residual error was small (RMS 0.06 m/s).

measurements (Figure 3.3). Measurements showed agreement with the flow meter readings; data were consistent with the line of identity (slope 0.98 P=0.39, offset 0.03 m/s P=0.1); and the residual error was small (RMS 0.06 m/s). 3D PC-SSFP data also showed a high correlation with 3D PC-GE data (r^2=0.99) and the line of regression was not significantly different from the line of identity (slope 1.06 P=0.20).

In vivo testing of blood velocities in the descending aorta in the long axis images was performed in eight subjects. Due to the long durations of the sequences, not all acquisitions were successfully completed in every subject, and one subject had no clear segment of the descending aorta running through the long axis mitral valve slab. Mean and peak velocities were compared between 3D PC-SSFP and 3D PC-GE (Figure 3.4). Both measures correlated well, with mean velocity r^2=0.79 and peak velocity r^2=0.93. Mean velocity showed a small significant bias of 0.91 cm/s (P=0.02).

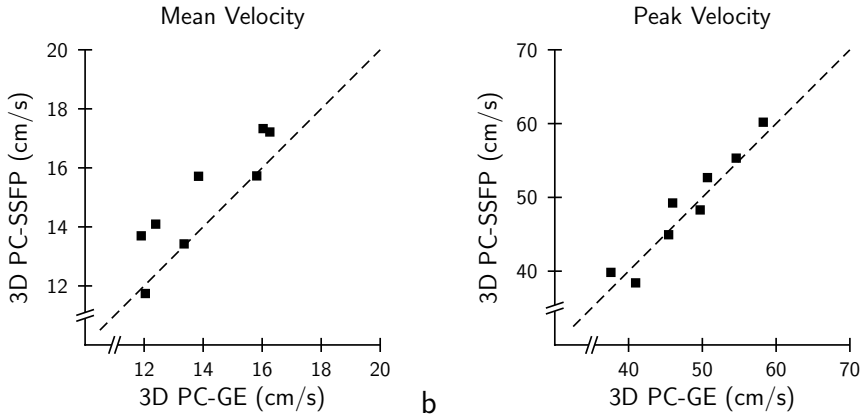

Figure 3.4: Velocity validation measurements in the descending aorta. Both mean and peak velocity correlated well between the two methods (respectively, r^2=0.79 and r^2=0.93), mean velocity showed a small bias of 0.91 cm/s.

Mitral Valve Imaging

Figure 3.5 shows typical long-axis images of the left atrium and ventricle as acquired with 3D PC-SSFP and 3D PC-GE. The lack of contrast, which was the initial problem, was evident in the 3D PC-GE images. At mid-systole (mitral valve closed), the border between the blood pool, and the myocardial wall showed almost no contrast, due to the absence of inflow of unsaturated spins (Figure 3.5, bottom left), while a distinct border was visible in the 3D PC-SSFP images (Figure 3.5, top left). These findings were confirmed by CNR measurements (Table 3.1). Both long-axis and short-axis systolic CNR values of 3D PC-SSFP were significantly higher compared to those for 3D PC-GE, except for short-axis diastolic images, where 3D PC-GE benefits maximally from inflow enhancement.

Velocity phase images of both sequences are also shown in Figure 3.5. These reflect a lower phase signal, a consequence of venc that was twice as high, as explained in Materials and Methods. This lower sensitivity could only be partially compensated for by the higher SNR of the SSFP, resulting in a VNR that was lower for 3D PC-SSFP except for the long-axis systolic data, where no difference was found (Ta-

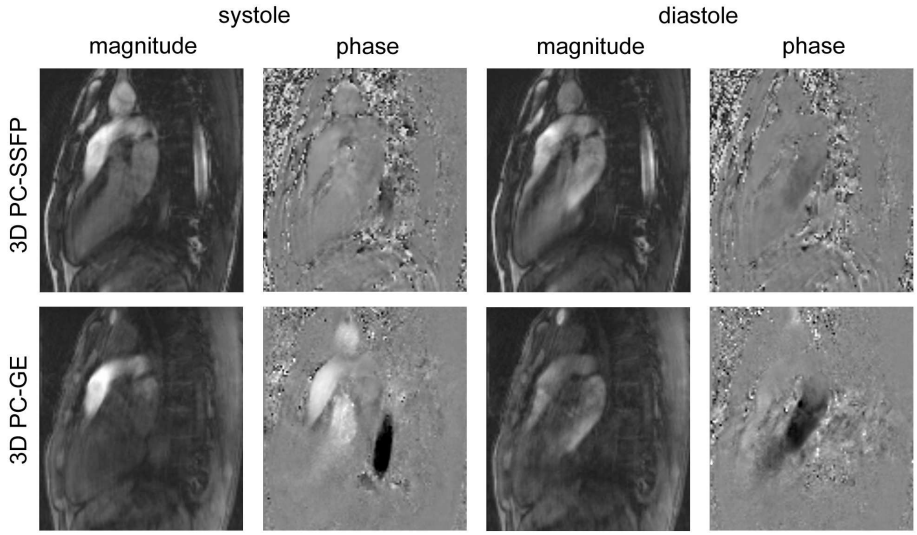

Figure 3.5: Typical 3D PCSSFP and 3D PC-GE long-axis images of the left atrium and ventricle (slice 4 of 8), in midsystole (200 msec after R peak) and at peak inflow in diastole (450 msec after R peak). 3D PC-SSFP magnitude images show better contrast than 3D PC-GE. Phase images of the SSFP show half the phase signal as a consequence of the method.

ble 3.1). However, 3D PC-SSFP used considerably shorter scantime, therefore VNR corrected for acquisition time, VNReff, shows a more balanced picture. Long-axis systole was now significantly improved for PC-SSFP, short-axis systole, and long-axis diastole showed no difference. Only short-axis diastole, where 3D PC-GE benefits maximally from inflow enhancement, had a lower VNReff (see Table 3.1).

Velocities at the level of the mitral valve were measured in nine subjects in long-axis orientation and in 10 subjects in short-axis orientation (Figure 3.6). Linear regression of the measurements showed no significant difference from the line of identity. However, mean velocity showed a poor correlation between 3D PC-SSFP and 3D PC-GE; the correlation in short axis was r^2=0.70 and in long axis r^2=0.56. In contrast to mean velocity, peak velocity showed a good correlation;

Table 3.1: Left ventricle CNR, VNR, and VNR_{eff} values of 3D PC-SSFP compared to 3D PC-GE during systole, 3D PC-SSFP showed a significant improvement in CNR value. Note the low CNR values in 3D PC-GE for both orientations. In short-axis diastole, when 3D PC-GE benefits maximally from inflow enhancement, the improvement by the 3D PC-SSFP technique was no longer significant. VNR values were worse in 3D PC-SSFP, but after correction for acquisition time (VNR_{eff}) both sequences have approximately similar values.

			3D PC-SSFP	3D PC-GE	P
CNR	short axis	systole	3.3	0.9	<0.01
		diastole	5.0	4.3	0.10
	long axis	systole	3.4	0.0	<0.01
		diastole	4.4	2.9	<0.01
VNR	short axis	systole	10.5	14.7	0.02
		diastole	14.2	27.7	<0.01
	long axis	systole	11.0	10.6	0.70
		diastole	13.3	20.7	0.01
VNR_{eff}	short axis	systole	4.6	4.4	0.20
		diastole	6.2	8.3	0.02
	long axis	systole	5.3	3.2	<0.01
		diastole	6.4	6.2	0.80

r^2=0.94 and r^2=0.81, for short and long axis, respectively. The low correlations in mean flow could not be explained by errors due to VNR values. Errors due to VNR constituted only 1% and 10% (short and long axis) of the residual variance in the correlation. BlandAltman analysis of intra- and interobserver variability showed that 3D PC-GE had generally a lower repeatability than 3D PC-SSFP. The BlandAltman plots of observer 1 are shown in Figure 3.7. The limits of repeatability estimated by the intra- and interobserver analyses are reported in Table 3.2.

The artifacts in the magnitude images were visually scored as follows for: short-axis 3D PC-SSFP, 1.6; 3D PC-GE, 1.8; long-axis scores were both 1.3. There were no significant differences between 3D

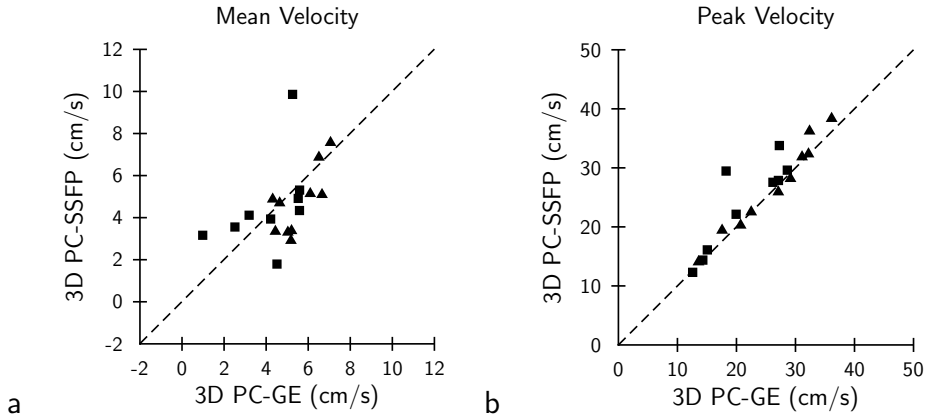

Figure 3.6: Velocity at the mitral valve level compared for both sequences, example from observer 1. Linear regression showed no significant difference from the line of identity; however, mean velocity showed poor correlation between the two methods; short-axis r^2=0.70 and long-axis r^2=0.56. Data of peak velocity had a good correlation: short-axis r^2=0.94 and long-axis r^2=0.81.

PC-SSFP and 3D PC-GE (short axis P=0.44, long axis P=0.81). The nature of the artifacts appeared to be somewhat different between the two sequences; however, 3D PC-SSFP had more flow artifacts whereas 3D PC-GE had more breathing artifacts (ghosting from subcutaneous fat in the chest wall).

3.4 Discussion

This study shows the feasibility of the combination of PC and a 3D SSFP sequence in the heart. After in vitro and in vivo testing, mitral valve imaging using this sequence was compared with the currently available sequence (3D PC-GE).

In vitro velocity measurements matched well with the regular flow meters and with 3D PC-GE measurements. In vivo measurements

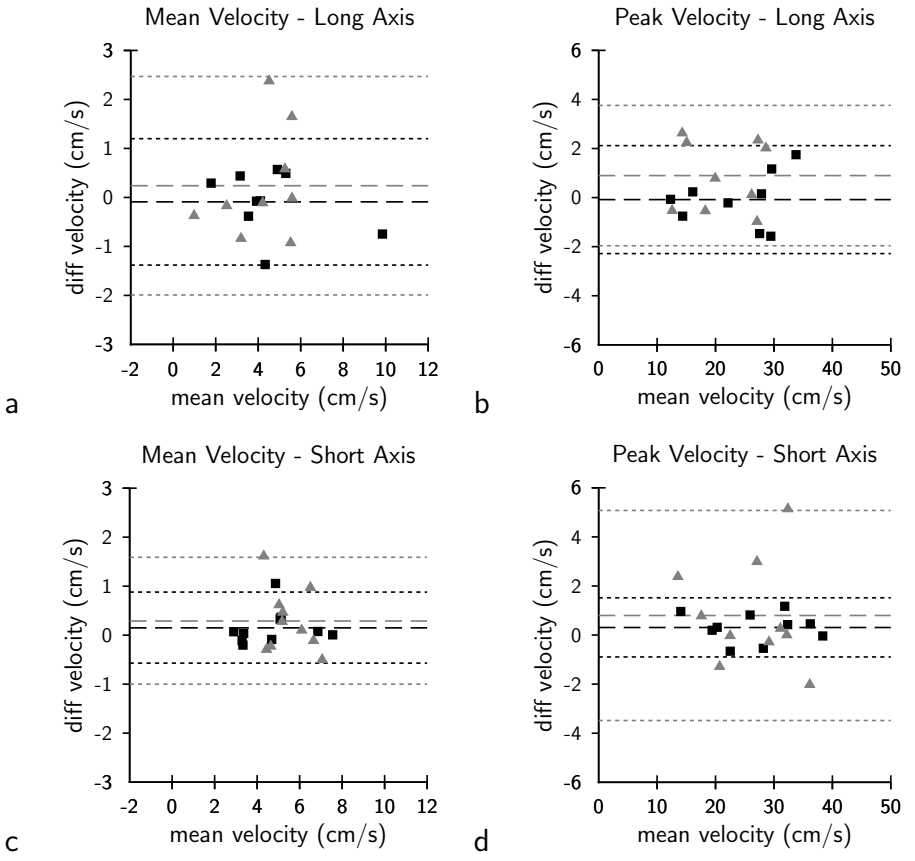

Figure 3.7: Bland-Altman plot on the intraobserver (obs. 1) repeatability of the velocity analysis. In all cases the repeatability of mean and peak velocity in both long- and short-axis orientation was lower in the 3D PC-GE data compared to the 3D PC-SSFP data.

Table 3.2: Limits of agreement for intra- and interobserver variability of both velocity and area measurements. 3D PC-GE limits are generally higher than those of 3D PC-SSFP.

				Limits of Agreement	
				3D PC-SSFP	3D PC-GE
velocities (cm/s)	short axis	average	observer 1	0.7	1.3
			observer 2	0.6	1.1
			observer 1 vs. 2	0.8	1.0
		peak	observer 1	1.2	4.3
			observer 2	3.1	4.0
			observer 1 vs. 2	4.2	4.8
	long axis	average	observer 1	1.3	2.2
			observer 2	1.1	2.7
			observer 1 vs. 2	2.4	1.9
		peak	observer 1	2.2	2.9
			observer 2	3.2	4.1
			observer 1 vs. 2	6.1	7.3
area (cm^2)	short axis		observer 1	1.3	1.3
			observer 2	1.3	3.9
			observer 1 vs. 2	2.3	6.5

showed a small but significant bias with 3D PC-GE. Overall et al. [16] reported a 10-20% bias between PC-SSFP and PCGE. They argued, with reference to a study by Summers et al. [31], that the bias was probably due to an underestimation of velocity by PC-GE. Their findings match our results in vivo, but not with our in vitro measurements. The cause of this difference should be investigated further.

Mitral valve imaging using 3D PC-SSFP showed good results. CNR improved significantly, as expected with an SSFP sequence [11, 13, 32]. VNR of 3D PC-SSFP was not as good as 3D PC-GE, except during systole in long-axis orientation, due to the higher venc necessary for PC-SSFP. As a result of the shorter TR of 3D PC-SSFP, the scan duration was shorter and VNR_{eff} was more or less similar in all the sequences.

At the mitral valve level, peak velocity measurements showed a

good correlation with 3D PC-GE, whereas mean velocity showed only a moderate correlation. Nevertheless, the correlation of the mean and peak velocity in the descending aorta was good, and the repeatability of 3D PC-SSFP was generally better than 3D PC-GE. Therefore, the moderate correlation between SSFP and GE at mean velocity through the mitral valve is not expected to be introduced by inaccuracies of the SSFP sequence itself. Using the VNR values it was shown that the statistical noise from the MR signal itself did not explain the above-mentioned moderate correlation.

The limits of agreement of repeated 3D PC-SSFP measurements were lower than the limits of agreement of repeated 3D PC-GE measurements of both intraobserver and interobserver studies on long- and short-axis mean and peak velocities and on short-axis area. As follows from these results, the poor repeatability of 3D PC-GE can more likely be explained by the limited CNR, as reliable contour drawing depends on image contrast. Based on these repeatability results, we think that the gain in CNR outweighs the reduction in absolute VNR.

Artifact sensitivity did not increase in the SSFP technique compared to GE imaging. The known artifacts in SSFP imaging due to high through-plane flow in 2D imaging are reduced in 3D imaging [27, 28]. However, breathing artifacts in 3D PC-GE are expected to be reduced when retrospective gating [33] is applied instead of prospective gating due to the more constant signal of subcutaneous fat in the chest wall throughout the cardiac cycle [34]. In contrast, flow artifacts in 3D PC-SSFP are less likely to be altered by retrospective triggering.

Working toward mitral valve flow quantification, a full 7D (3D spatial, 3D flow and time) acquisition would be the next step [5]. For this study we used only one direction of velocity sensitivity because we wanted to make multiple comparisons, which would not be possible with the longer acquisition times of a 7D approach. The 3D PC-SSFP allows the use of the minimal TR, whereas for GE a higher TR had to be chosen to enable some inflow enhancement, resulting in a reduction of acquisition time for 3D PC-SSFP. Parallel imaging techniques, such as k-t BLAST and k-t SENSE [35], are interest-

ing options for the further reduction of acquisition times. Another necessity for accurate flow quantification through the mitral valve, especially in cases of mitral regurgitation, is full coverage of the diastolic phase. This requires the implementation of retrospective cardiac gating [29].

There are also some specific issues to be addressed in the quest for mitral valve flow quantification. In patients with mitral insufficiency, high-velocity regurgitation jets are often observed [1, 16], introducing another technical challenge. Artifact behavior of 3D PC-SSFP in the presence of regurgitation jets is hard to predict, but might be an issue [16, 36, 37]. As the phase-velocity behavior of the 3D PC-SSFP sequence is only linear over a finite range [16], velocity unwrapping [38] as might occur in high velocity jets is not straightforward. Further research on patients with mitral insufficiency is desired. The range of linearity is influenced by the shim [16], but this was not specifically investigated in this study.

Although this study was directed at mitral flow quantification, the lack of contrast in 3D PC-GE applies in general to the whole heart [9, 10]. The results of this study, ie, the gain in CNR, are in line with the well-known advantages of regular (non-PC) SSFP sequences in the heart [11, 13]. Therefore, it is likely that the results of this study can be applied to a broader view, beyond the mitral valve alone. The sequence might very well be used for other flow quantification purposes in the heart. In locations where there is enough inflow of unsaturated spins, such as the aorta, the gain in CNR is not expected to be significant [19, 39, 40].

In conclusion, this study showed the successful implementation of a 3D velocity quantification sequence: 3D PC-SSFP. Mitral valve images demonstrated significant improvement in blood-myocardium contrast, and velocity measurements showed better reproducibility with 3D PC-SSFP.

3.5 Bibliography

[1] L. Sondergaard, F. Stahlberg, and C. Thomsen. Magnetic resonance imaging of valvular heart disease. *Journal of Magnetic Resonance Imaging*, 10(5):

627–638, 1999.

[2] C.M. Tribouilloy, M. Enriquez-Sarano, H.V. Schaff, T.A. Orszulak, K.R. Bailey, A.J. Tajik, and R.L. Frye. Impact of preoperative symptoms on survival after surgical correction of organic mitral regurgitation - rationale for optimizing surgical indications. *Circulation*, 99(3):400–405, 1999.

[3] P.J. Kilner, P.D. Gatehouse, and D.N. Firmin. Flow measurement by magnetic resonance: A unique asset worth optimising. *Journal of Cardiovascular Magnetic Resonance*, 9(4):723–728, 2007.

[4] S. Kozerke, J. Schwitter, E.M. Pedersen, and P. Boesiger. Aortic and mitral regurgitation: quantification using moving slice velocity mapping. *Journal of Magnetic Resonance Imaging*, 14(2):106–112, 2001.

[5] P.G. Walker, K. Houlind, C. Djurhuus, W.Y. Kim, and E.M. Pedersen. Motion correction for the quantification of mitral regurgitation using the control volume method. *Magnetic Resonance in Medicine*, 43(5):726–733, 2000.

[6] D.N. Firmin, G.L. Nayler, R.H. Klipstein, S.R. Underwood, R.S.O. Rees, and D.B. Longmore. Invivo validation of MR velocity imaging. *Journal of Computer Assisted Tomography*, 11(5):751–756, 1987.

[7] G.L. Nayler, D.N. Firmin, and D.B. Longmore. Blood-flow imaging by cine magnetic-resonance. *Journal of Computer Assisted Tomography*, 10(5):715–722, 1986.

[8] N.J. Pelc, F.G. Sommer, K.C.P. Li, T.J. Brosnan, R.J. Herfkens, and D.R. Enzmann. Quantitative magnetic-resonance flow imaging. *Magnetic Resonance Quarterly*, 10(3):125–147, 1994.

[9] E.M. Haacke, R.W. Brown, M.R. Thompson, and R. Venkatesan. *MR angiography and flow quantification.*, pages 703–740. John Wiley & Sons, New York, 1999.

[10] J.H. Gao and J.C. Gore. NMR signal from flowing nuclei in fast gradient-echo pulse sequences with refocusing. *Physics in Medicine and Biology*, 39 (12):2305–2318, 1994.

[11] K. Scheffler and S. Lehnhardt. Principles and applications of balanced SSFP techniques. *European Radiology*, 13(11):2409–2418, 2003.

[12] R. Nezafat, D. Herzka, C. Stehning, D.C. Peters, K. Nehrke, and W.J. Manning. Inflow quantification in three-dimensional cardiovascular MR imaging. *Journal of Magnetic Resonance Imaging*, 28(5):1273–1279, 2008.

[13] J. Barkhausen, S.G. Ruehm, M. Goyen, T. Buck, G. Laub, and J.F. Debatin. MR evaluation of ventricular function: True fast imaging with steady-state precession versus fast low-angle shot cine MR imaging: Feasibility study. *Radiology*, 219(1):264–269, 2001.

[14] A.E. Stillman, N. Wilke, and M. Jeroschherold. Use of an intravascular T1 contrast agent to improve MR cine myocardial-blood pool definition in men. *Journal of Magnetic Resonance Imaging*, 7(4):765–767, 1997.

[15] M. Markl, M.T. Alley, and N.J. Pelc. Balanced phase-contrast steady-state free precession (PC-SSFP): A novel technique for velocity encoding by gra-

dient inversion. *Magnetic Resonance in Medicine*, 49(5):945–952, 2003.

[16] W.R. Overall, D.G. Nishimura, and B.S. Hu. Fast phase-contrast velocity measurement in the steady state. *Magnetic Resonance in Medicine*, 48(5): 890–898, 2002.

[17] V.M. Pai. Phase contrast using multiecho steady-state free precession. *Magnetic Resonance in Medicine*, 58(2):419–424, 2007.

[18] F. Santini, S.G. Weetzel, and K. Scheffler. Three-dimensional time-resolved flow quantification with balanced SSFP. *Proc.Intl.Soc.Mag.Reson.Med.*, 16: 2878, 2008.

[19] M.P. Rolf, M.B.M. Hofman, J.P.A. Kuijer, V.M. Pai, A. Greiser, A.C. van Rossum, and R.M. Heethaar. Extrinsic multiecho phase-contrast SSFP: evaluation on cardiac output measurements. *Magnetic Resonance Imaging*, 27 (3):385–392, 2009.

[20] G.D.O. Lowe, F.G.R. Fowkes, J. Dawes, P.T. Donnan, S.E. Lennie, and E. Housley. Blood-viscosity, fibrinogen, and activation of coagulation and leukocytes in peripheral arterial-disease and the normal population in the edinburgh artery study. *Circulation*, 87(6):1915–1920, 1993.

[21] C.L. Dumoulin, S.P. Souza, M.F. Walker, and W. Wagle. 3-dimensional phase-contrast angiography. *Magnetic Resonance in Medicine*, 9(1):139–149, 1989.

[22] L. Wigstrom, L. Sjoqvist, and B. Wranne. Temporally resolved 3D phase-contrast imaging. *Magnetic Resonance in Medicine*, 36(5):800–803, 1996.

[23] M. Markl. Time resolved three dimensional phase contrast MRI. *Journal of Magnetic Resonance Imaging*, 18(3):396, 2003.

[24] B.A. Jung, J. Hennig, and K. Scheffler. Single-breathhold 3d-trueFISP cine cardiac imaging. *Magnetic Resonance in Medicine*, 48(5):921–925, 2002.

[25] S. Kozerke, J. Tsao, R. Razavi, and P. Boesiger. Accelerating cardiac cine 3D imaging using k-t BLAST. *Magnetic Resonance in Medicine*, 52(1):19–26, 2004.

[26] T. Ebbers, L. Wigstrom, A.F. Bolger, J. Engvall, and M. Karlsson. Estimation of relative cardiovascular pressures using time-resolved three-dimensional phase contrast MRI. *Magnetic Resonance in Medicine*, 45(5): 872–879, 2001.

[27] S. Kozerke, J.M. Hasenkam, E.M. Pedersen, and P. Boesiger. Visualization of flow patterns distal to aortic valve prostheses in humans using a fast approach for cine 3D velocity mapping. *Journal of Magnetic Resonance Imaging*, 13(5):690–698, 2001.

[28] J.W. Lankhaar, M.B.M. Hofman, J.T. Marcus, J.J.M. Zwanenburg, T.J.C. Faes, and A. Vonk-Noordegraaf. Correction of phase offset errors in main pulmonary artery flow quantification. *Journal of Magnetic Resonance Imaging*, 22(1):73–79, 2005.

[29] C.D. Constantinides, E. Atalar, and E.R. McVeigh. Signal-to-noise measurements in magnitude images from NMR phased arrays. *Magnetic Resonance*

in Medicine, 38(5):852–857, 1997.

[30] T.E. Conturo and G.D. Smith. Signal-to-noise in phase-angle reconstruction - dynamic-range extension using phase reference offsets. *Magnetic Resonance in Medicine*, 15(3):420–437, 1990.

[31] P.E. Summers, M. Drangova, A. Papadaki, D.W. Holdsworth, and B.K. Rutt. Multi-site comparison of accuracy, linearity, and precision in MR flow measurements. *Proc.Intl.Soc.Mag.Reson.Med.*, 09:370, 2001.

[32] Y. Zur, S. Stokar, and P. Bendel. An analysis of fast imaging sequences with steady-state transverse magnetization refocusing. *Magnetic Resonance in Medicine*, 6(2):175–193, 1988.

[33] G.W. Lenz, E.M. Haacke, and R.D. White. Retrospective cardiac gating - a review of technical aspects and future-directions. *Magnetic Resonance Imaging*, 7(5):445–455, 1989.

[34] D. Li, C.B. Paschal, E.M. Haacke, and L.P. Adler. Coronary-arteries - 3-dimensional mr-imaging with fat saturation and magnetization transfer contrast. *Radiology*, 187(2):401–406, 1993.

[35] J. Tsao, P. Boesiger, and K.P. Pruessmann. k-t BLAST and k-t SENSE: dynamic MRI with high frame rate exploiting spatiotemporal correlations. *Magnetic Resonance in Medicine*, 50(5):1031–1042, 2003.

[36] O. Bieri and K. Scheffler. Flow compensation in balanced SSFP sequences. *Magnetic Resonance in Medicine*, 54(4):901–907, 2005.

[37] M. Markl and N.J. Pelc. On flow effects in balanced steady-state free precession imaging: Pictorial description, parameter dependence, and clinical implications. *Journal of Magnetic Resonance Imaging*, 20(4):697–705, 2004.

[38] M. Jenkinson. Fast, automated, N-dimensional phase-unwrapping algorithm. *Magnetic Resonance in Medicine*, 49(1):193–197, 2003.

[39] W.G. Hundley, H.F. Li, L.D. Hillis, B.M. Meshack, R.A. Lange, J.E. Willard, C. Landau, and R.M. Peshock. Quantitation of cardiac-output with velocity-encoded, phase-difference magnetic-resonance-imaging. *American Journal of Cardiology*, 75(17):1250–1255, 1995.

[40] J. Lotz, C. Meier, A. Leppert, and M. Galanski. Cardiovascular flow measurement with phase-contrast MR imaging: Basic facts and implementation. *Radiographics*, 22(3):651–671, 2002.